Arab J Sci Eng (2016) 41:3571–3586
DOI 10.1007/s13369-016-2201-8

RESEARCH ARTICLE - ELECTRICAL ENGINEERING

A Modified Disturbance Rejection Mechanism in Sliding Mode State Observer for Sensorless Induction Motor Drive

S. Mohan Krishna[1] · **J. L. Febin Daya**[1]

Received: 27 July 2015 / Accepted: 11 May 2016 / Published online: 4 June 2016
© King Fahd University of Petroleum & Minerals 2016

Abstract This paper presents a modified sliding mode state observer for sensorless vector-controlled induction motor drive. The objective is to improve the dynamic performance of the sensorless drive subjected to parameter uncertainty, fault and disturbances. The sensorless drive along with the proposed observer is modeled and built in Simulink, and the dynamic behavior is obtained for different test cases such as flux-weakening region, variations in commanded speed and torque, low-speed operation and under faulty operation mode subjected to an electrical fault in the inverter. The conventional disturbance rejection mechanism is modified by constraining the estimated disturbance along with the stator current error in the sliding surface, thereby increasing the ability of the observer to reject the effect of the external load on the tracking performance. Extensive simulation results prove that the modified observer has a wide speed bandwidth compared to the conventional observer along with superior tracking, disturbance rejection characteristics and torque holding capability.

Keywords Parameter estimation · Model Reference Adaptive Systems (MRAS) · Disturbance rejection · Sliding mode · Flux weakening · Vector control

List of symbols

$i^{s}_{ds}, i^{s}_{qs}, i^{r}_{dr}, i^{r}_{qr}$	d- and q-axis stator and rotor currents in the stationary and rotating reference frame
v^{s}_{ds}, v^{s}_{qs}	d- and q-axis stator voltages in stationary reference frame
T_r	Rotor time constant
R_s, R_r	Stator and rotor resistance
σ	Leakage reactance
L_r, L_m, L_s	Rotor, magnetizing and stator self inductance
L_{ls}, L_{lr}	Stator and rotor leakage inductances
$\omega_r, \hat{\omega}_r, \omega^*, \omega_{bsync}$	Actual rotor speed, estimated rotor speed, speed reference, base synchronous speed
$\psi^{s}_{ds}, \psi^{s}_{qs}, \psi^{s}_{dr}, \psi^{s}_{qr}$	d-axis and q-axis stator and rotor flux linkages in stationary reference frame
$\hat{\varphi}_d, \hat{\varphi}_q$	d-axis and q-axis estimated rotor flux linkages
$\theta_f, \theta_{sl}, \theta_r$	Field angle, slip angle and rotor angle
T^*_e	Reference electromagnetic torque
i^*_{ds}, i^*_{qs}	d-axis and q-axis stator currents in synchronously rotating reference frame
$i^*_{as}, i^*_{bs}, i^*_{cs}$	3 phase reference currents

1 Introduction

The introduction of power semiconductor switching converters has led to increased usage and deployment of variable-speed drives. Inverter fed induction motor continues to be the workhorse of the industry owing to its robustness,

✉ S. Mohan Krishna
smk87.genx@gmail.com

[1] School of Electrical Engineering, VIT University, Chennai Campus, Chennai, Tamil Nadu, India

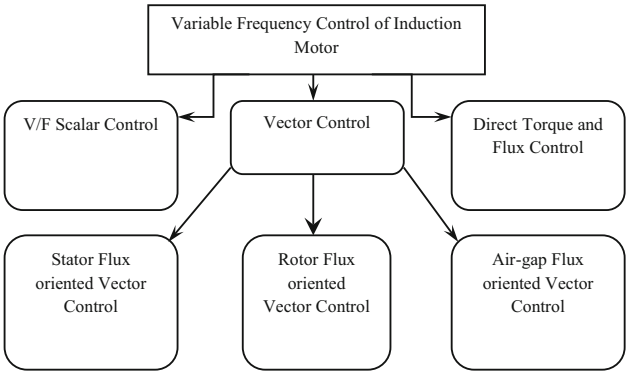

Fig. 1 Variable frequency control strategies

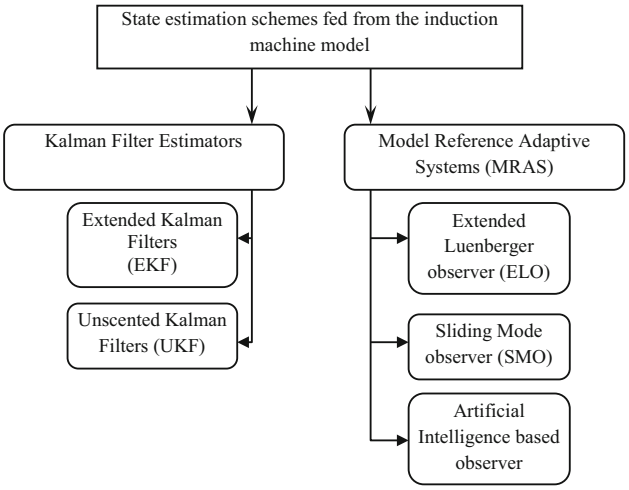

Fig. 2 Speed estimation from machine model

cost, less maintenance and a wide speed range and torque holding capability. There are several strategies for variable frequency control of induction motor as given in Fig. 1. The field-oriented control or vector control has an advantage of better dynamic performance by means of independent torque and flux control. A separately excited DC machine-like performance can be obtained by achieving an orthogonal orientation of torque and flux. Therefore, an almost linear torque response characteristic similar to that of a separately excited DC motor can be obtained [1]. In the decoupled model of the induction motor, the field orientation is forced by making the flux vector align along the d-axis of the reference frame. Generally, the rotor flux vector is aligned with the d-axis as compared to the air gap and stator flux vectors to overcome the effect of coupling.

To enforce field orientation, there were two methods identified which was the direct and indirect rotor flux-oriented vector control. In the former, to achieve the magnitude and flux angle for field orientation, Hall effect sensors were mounted in the air gap which in turn required a modified machine. Moreover, the sensitivity of the sensors implied behaved contrary to the robustness of the induction motor. In the latter, the field orientation was achieved by thrusting a slip frequency derived from the rotor dynamic equation, thereby eliminating the provision of Hall effect or flux sensors. However, it required a speed sensor mounted on the shaft of the induction motor to generate the control signals. This again meant additional electronics, wiring, cost and mounting space. Many researchers focused on implementing a vector control mechanism without the need for speed sensors over the last few decades [2]. This gave rise to the concept of sensorless vector control of induction motor drives.

For rotor speed and other parameter estimation, sensorless vector control schemes either made use of the magnetic saliencies or the machine model. Though the parameter estimation through the former, such as rotor slotting, rotor slot harmonics, was considered an accurate form of measurement and parameter independent, they introduced measurement delays and were found inadequate for closed-loop feedback control. The latter, comprising of machine model-based speed estimation schemes, were more popular, had less computational space and were easy to implement [3]. But they were parameter dependent, and therefore, joint estimation of the rotor speed along with other significant parameters had to be done to prevent any mismatch under all operating conditions [4–7]. Besides, there is a necessity for parameter adaptation for a wide range high-performance sensorless vector control drive. Adaptive parameter estimation schemes fed from the machine model occupied more research space for their ability to adapt themselves to the controlled system. The general principle behind these schemes was the MRAS. It has been used in various forms for state estimation of the induction motor as shown in Fig. 2. The extended luenberger sliding mode and artificial intelligence-based state observers are more popular owing to their estimation performance for wide speed bandwidth, tracking capability and disturbance rejection [8–12]. There are several methods involving joint or simultaneous estimation of rotor speed and resistive parameters like stator and rotor resistances or inductive parameters like the leakage inductance which are strongly dependent on the flux level and the load [13,14]. Schemes involving disturbance torque estimation have also been implemented in order to reject the effect of the load torque on the estimation performance of the observer [15–18].

This paper implements a sliding mode luenberger observer for joint estimation of rotor speed and disturbance torque for sensorless vector-controlled induction motor drive. The disturbance torque is estimated by exploiting the mechanical model of the induction motor and is then modeled into the observer state dynamic equation. Two disturbance rejection mechanisms, based on the placement of the estimated disturbance in the observer state dynamic equation, are compared.

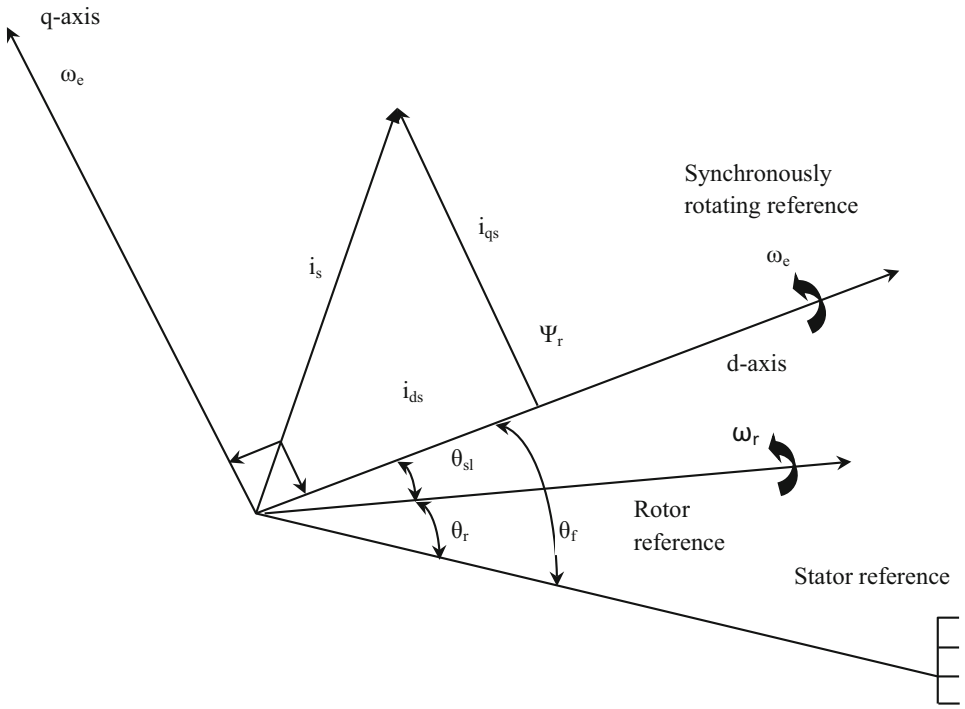

Fig. 3 Phasor representation of field-oriented control

An effort is made to modify the conventional disturbance rejection mechanism by constraining the estimated disturbance along with the stator current error in the sliding surface. The supremacy and the dynamic performance of the modified disturbance rejection mechanism over the conventional one are validated under different test cases involving the flux-weakening region, speed and torque perturbations and low-speed operation and presented. Also, since inverter faults contribute almost 38 % of the faults in variable-speed drives, the performance of the observers' in the faulty operation mode for input DC-link voltage disturbance is also presented. The observer and the closed-loop vector controller models along with the motor are modeled, built and simulated using MATLAB/Simulink blocksets, and the results are validated.

2 Indirect Rotor Flux-Oriented Control and MRAS

The essence of field-oriented control or the vector control involves controlling the components of the stator currents of the motor which are represented by a vector in the d–q coordinate system in a rotating reference frame. In indirect vector control strategy, the field orientation is established by means of a slip frequency derived from the rotor dynamic equations (current model), which required a knowledge of the shaft speed. The concept is illustrated in the form of phasor diagram as shown in Fig. 3.

Consider the decoupled model of the induction motor in the reference frame rotating at synchronous speed, the implication of field-oriented control is to force i_{ds} component (field producing) of the stator current with the rotor flux and the i_{qs} component (torque producing) of the stator current orthogonal to i_{ds}. This decouples the torque and flux control loops and enables independent control of torque and flux.

The configuration of MRAS-based parameter estimation scheme is shown in Fig. 4.

It comprises of the reference and the adaptive models fed from the terminal quantities of the motor. The reference model is the motor model, and the adaptive model consists of the sliding mode luenberger state observer. The adaptive mechanism is used to force convergence between the actual and estimated outputs. Hence, this gives rise to an optimization criterion, i.e., to ensure minimization of the error vector to zero such that the estimated quantities converge to their actual values.

$$C = \int_0^{\mathrm{T}} e^2 \mathrm{d}t \tag{1}$$

C being the optimization criterion, and the error vector to be constrained is given by,

$$e = Y_{\mathrm{ref}} - Y_{\mathrm{adap}} \tag{2}$$

where Y_{ref} and Y_{adap} are the reference model and adaptive model outputs, respectively. This paper makes use of MRAS-based sliding mode observer for rotor speed and disturbance torque estimation. The presence of a sliding surface is to constrain the system state to ensure better tracking

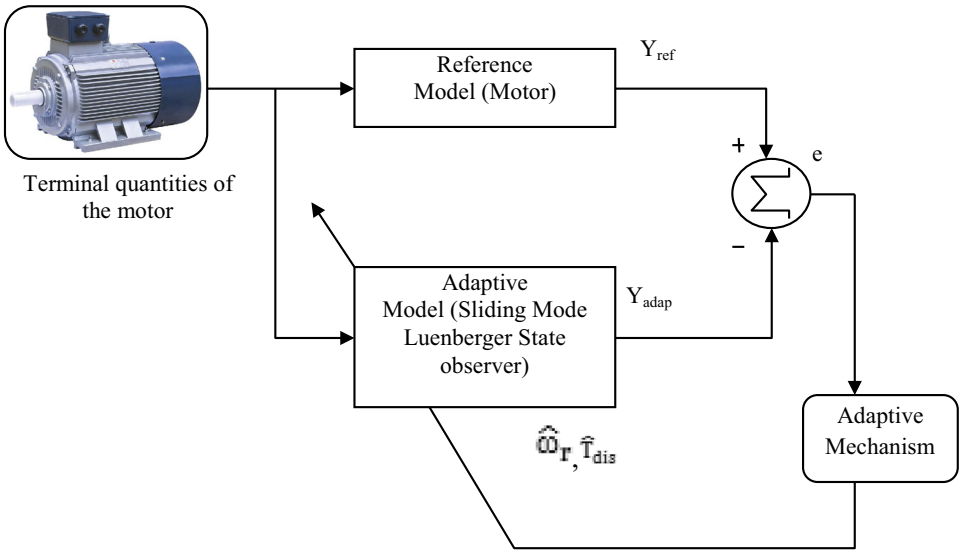

Fig. 4 MRAS-based state estimation

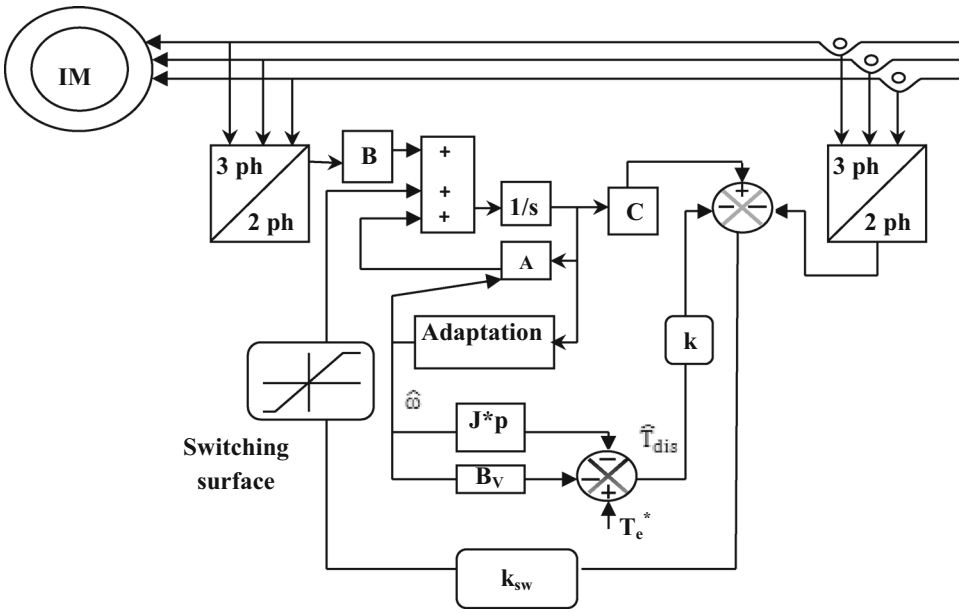

Fig. 5 Proposed sliding mode rotor speed and disturbance torque observer

and dynamic performance. The rotor speed is determined by a proportional–integral (PI)-based adaptation mechanism based on the Lyapunov theory to ensure stability of the drive system at wide speed ranges. The disturbance torque is determined by making use of the mechanical model and is incorporated into the observer structure.

3 Modeling of the Sliding Mode Luenberger State Observer and Vector Controller

The modified adaptive pseudo-reduced-order observer (APRO) using a switching surface is shown in Fig. 5, where 'A' is the system matrix, the symbol '^' indicates estimated quantities, 'X' consists of the state variables which comprise the direct and quadrature axes stator currents and rotor fluxes, 'k_{sw}' is the reduced-order observer switching gain matrix, chosen such that the eigenvalues of the observer are proportional to the eigenvalues of the machine to ensure stability under normal operating conditions. 'J' is the moment of inertia, 'p' is the differential operator, 'B_V' is the viscous friction coefficient, 'T_e^*' is the reference model electromagnetic torque, '$\hat{T}_{dis}$' is the estimated disturbance torque, which is the difference between reference model and the adaptive model electromagnetic torque, and 'k' is an arbitrary positive gain.

The structure of the above observer scheme with motor model, disturbance torque estimation and compensation along with the current regulated vector controller is shown below:

3.1 MRAS-Based Observer

The state space equations are used to characterize the motor and the observer model as it is easier to express control and estimation algorithms [19,20].

3.1.1 Motor Model (Reference Model)

The equations depicting the reference model of the MRAS-based observer are as follows:

$$\frac{\mathrm{d}x}{\mathrm{d}t} = [A]\,x + [B]\,u \tag{3}$$

$$y = [C]\,x \tag{4}$$

where

$$x = \left[i_{\mathrm{ds}}^{\mathrm{s}}, i_{\mathrm{qs}}^{\mathrm{s}}, \psi_{\mathrm{dr}}^{\mathrm{s}}, \psi_{\mathrm{qr}}^{\mathrm{s}}\right]^{\mathrm{T}}, \quad A = \begin{bmatrix} A_{11} & A_{12} \\ A_{21} & A_{22} \end{bmatrix},$$

$$B = \left[\frac{1}{\sigma L_{\mathrm{s}}} I \quad 0\right]^{\mathrm{T}},$$

$$C = [I, 0],$$

$$u = \left[v_{\mathrm{ds}}^{\mathrm{s}} v_{\mathrm{qs}}^{\mathrm{s}}\right]^{\mathrm{T}}$$

$$I = \begin{bmatrix} 1 & 0 \\ 0 & 1 \end{bmatrix},$$

$$J = \begin{bmatrix} 0 & -1 \\ 1 & 0 \end{bmatrix},$$

$$A_{11} = -\left[\frac{R_{\mathrm{s}}}{\sigma L_{\mathrm{s}}} + \frac{1-\sigma}{\sigma T_{\mathrm{r}}}\right] I = a_{\mathrm{r}11} I,$$

$$A_{12} = \frac{L_{\mathrm{m}}}{\sigma L_{\mathrm{s}} L_{\mathrm{r}}}\left[\frac{1}{T_{\mathrm{r}}} I - \omega_{\mathrm{r}} J\right] = a_{\mathrm{r}12} I + a_{\mathrm{i}12} J,$$

$$A_{21} = \frac{L_{\mathrm{m}}}{T_{\mathrm{r}}} I = a_{\mathrm{r}21} I,$$

$$A_{22} = \frac{-1}{T_{\mathrm{r}}} I + \omega_{\mathrm{r}} J = a_{\mathrm{r}22} I + a_{\mathrm{i}22} J,$$

3.1.2 Disturbance Torque Estimate

Making use of the mechanical model, the disturbance torque is estimated by the following equation. It is a function of the actual and estimated speed and flux.

$$\widehat{T}_{\mathrm{dis}} = T_{\mathrm{e}}^{*} - J\frac{\mathrm{d}\hat{\omega}}{\mathrm{d}t} - B_{\mathrm{V}}\hat{\omega} \tag{5}$$

where $\hat{\omega}$ is the estimated speed.

3.1.3 APRO 1: Conventional Disturbance Rejection Mechanism (Adaptive Model)

The estimated disturbance torque is incorporated into the observer state dynamic equation utilizing a sliding surface as shown. It is a variable structure control strategy whose purpose is to constrain the system trajectory to the sliding surface. It should be chosen such that the Lyapunov function candidate V (a scalar function of S), used for the derivation of the adaptive mechanism, and its derivative satisfy the Lyapunov stability criteria given by Slotine and Li [21],

$$\dot{V}(S) = S(x)\,\dot{S}(x) \tag{6}$$

The control rule is given by:

$$u(t) = u_{\mathrm{eq}}(t) + u_{\mathrm{sw}}(t) \tag{7}$$

where the control vector is denoted by $u(t)$, and $u_{\mathrm{eq}}(t)$ and $u_{\mathrm{sw}}(t)$ represent the equivalent control vector and the switching vector, respectively. In order to satisfy the stability condition, the switching vector is determined as follows [22]:

$$u_{\mathrm{sw}}(t) = \eta\,\mathrm{sign}(S(x,t)) \tag{8}$$

where

$$\mathrm{sign}(S) = \begin{cases} -1 & \text{for } S < 0 \\ 0 & \text{for } S = 0 \\ +1 & \text{for } S > 0 \end{cases}$$

where η is the switching control gain, which is chosen in such a way so as to make (6) negative definite and also have a large enough value to reject the effect of the external disturbance. The introduction of the sliding surface also increases the nonlinearity of the system, giving rise to chattering phenomenon. Therefore, a saturation function with a boundary layer of width (Φ) is used to relieve the effect of the unwanted chattering phenomenon by replacing sign(S) with sat(S/Φ) which is expressed as follows:

$$\mathrm{sat}(S/\Phi) = \begin{cases} \mathrm{sign}\left(\frac{S}{\Phi}\right) & \text{if } \left|\left(\frac{S}{\Phi}\right)\right| \geq 1 \\ \left(\frac{S}{\Phi}\right) & \text{if } \left|\left(\frac{S}{\Phi}\right)\right| < 1 \end{cases} \tag{9}$$

The equations describing the observer with the disturbance modeled into the observer state dynamic equation are shown below:

$$\frac{\mathrm{d}\hat{x}}{\mathrm{d}t} = \left[\hat{A}\right]\hat{x} + [B]\,u + k_{\mathrm{sw}}\mathrm{sat}\left(\hat{i}_{\mathrm{s}} - i_{\mathrm{s}}\right) + \hat{d} \tag{10}$$

where the sliding surface $s = \hat{i}_s - i_s$ and $\hat{d} = k\hat{T}_{dis}$ and

$$\hat{y} = [C]\hat{x} \tag{11}$$

$\hat{i}_s$ = estimated value of stator current,

i_s = measured value of stator current

$$\hat{A} = \begin{bmatrix} A_{11} & \hat{A}_{12} \\ A_{21} & \hat{A}_{22} \end{bmatrix},$$

$$\hat{A}_{12} = \frac{L_m}{\sigma L_s L_r}\left[\frac{1}{T_r} I - \hat{\omega}_r J\right] = a_{r12} I + \hat{a}_{i12} J,$$

$$\hat{A}_{22} = \frac{-1}{T_r} I + \hat{\omega}_r J = a_{r22} I + \hat{a}_{i22} J$$

'k_{sw}' is the reduced-order switching gain matrix designed for stabilizing (7). The pseudo-reduced-order gain matrix is chosen as follows:

$$k_{sw} = \begin{bmatrix} k_1 & k_2 \\ -k_2 & k_1 \end{bmatrix}^T \tag{12}$$

On the basis of pole placement technique, the switching gain matrix is determined, in order to ensure the convergence of the state of the observer with that of the motor. For faster and more rapid convergence, the eigenvalues of the observer are chosen relatively more negative than the eigenvalues of the motor. Therefore,

$$k_1 = (m-1)\, a_{r11} \tag{13}$$

$$k_2 = k_p, k_p \geq -1 \tag{14}$$

'm' is arbitrarily chosen and k_1 depends on the motor parameters.

3.1.4 APRO 2: Modified Disturbance Rejection Mechanism (Adaptive Model)

Here, the state dynamic equation of the conventional observer is modified by relocating the estimated disturbance torque into the sliding surface. Therefore, the disturbance torque estimate along with the stator current error is constrained within the sliding surface.

$$\frac{d\hat{x}}{dt} = \left[\hat{A}\right]\hat{x} + [B]\, u + k_{sw}\text{sat}\left(\hat{i}_s - i_s - \hat{d}\right) \tag{15}$$

Now, the sliding surface becomes $s = \hat{i}_s - i_s - \hat{d}$ and $\hat{d} = k\hat{T}_{dis}$ and

$$\hat{y} = [C]\,\hat{x} \tag{16}$$

3.1.5 Adaptive Mechanism

The Lyapunov stability criterion is used for deriving the adaptive mechanism with the following function candidate:

$$V = e^T e + \frac{\left(\hat{\omega}_r - \omega_r\right)^2}{\lambda} \tag{17}$$

where λ is a positive constant.

Taking the derivative of V with respect to t as shown:

$$\frac{dv}{dt} = e^T\left[(A + GC)^T + (A + GC)\right]e - \frac{2\Delta\omega_r\left(e_{ids}\hat{\varphi}^s_{qr} - e_{iqs}\hat{\varphi}^s_{dr}\right)}{c} + \frac{2\Delta\omega_r}{\lambda}\frac{d\hat{\omega}_r}{dt} \tag{18}$$

where

$$e_{ids} = i^s_{ds} - \hat{i}^s_{ds},$$

$$e_{iqs} = i^s_{qs} - \hat{i}^s_{qs}$$

By equalizing the second term with the third term, the adaptive mechanism for speed is obtained:

$$\frac{d\hat{\omega}_r}{dt} = \frac{\lambda}{c}\left(e_{ids}\hat{\varphi}^s_{qr} - e_{iqs}\hat{\varphi}^s_{dr}\right) \tag{19}$$

where c is an arbitrary positive constant.

3.2 Vector Controller

Since the hysteresis band current regulation is not dependent on load parameters and owing to its fast response current loop, it is considered in this paper. The vector control concept makes use of rotor dynamics as it involves phasor control of the rotor flux. A proportional–integral controller processes the error between the estimated speed and the speed command and generates the reference torque as shown:

$$e_c = \hat{\omega}_r - \omega^* \tag{20}$$

$$T^*_e = e_c\left[k_p + (k_i/s)*T_s\right] \tag{21}$$

where e_c is the speed error to be processed by the discrete PI controller, k_p and k_i are the proportional and integral gains, and T_s is the sampling time for the closed-loop algorithm. The rotor flux is assumed to be constant, and for speeds ranging above the base synchronous speed in the field weakening region, it is taken as a function of the speed.

$$\psi_r = 0.96 \quad \text{If } \hat{\omega}_r < \omega_{bsync} \tag{22}$$

$$\psi_r = 0.96*\left(\frac{\hat{\omega}_r}{\omega_{bsync}}\right) \quad \text{If } \hat{\omega}_r > \omega_{bsync} \tag{23}$$

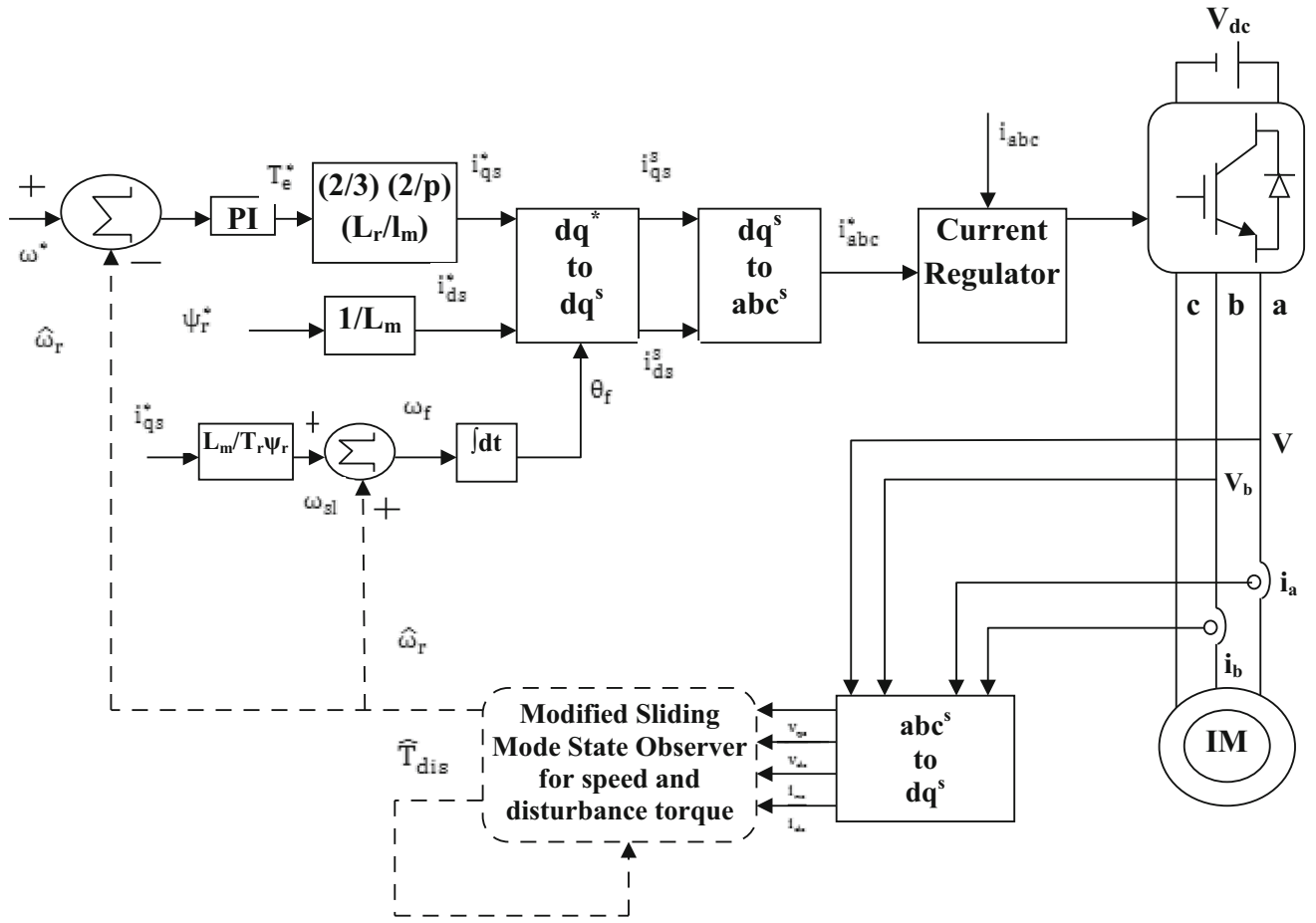

Fig. 6 Sensorless drive system with modified observer

The orthogonal flux and torque-producing components of the current are estimated from the reference torque and the rotor flux.

$$i_{\mathrm{ds}}^{*} = \left(\frac{\psi_{\mathrm{r}}}{L_{\mathrm{m}}}\right)\left[1 + \frac{dT_{\mathrm{r}}}{dT_{\mathrm{s}}}\right] \tag{24}$$

$$i_{\mathrm{qs}}^{*} = \left(\frac{2}{3}\right)\left(\frac{2}{P}\right)\left(\frac{L_{\mathrm{r}}}{L_{\mathrm{m}}}\right)\left(\frac{T_{\mathrm{ref}}}{\psi_{\mathrm{r}}}\right) \tag{25}$$

From the slip speed, the field angle is determined.

$$\theta_{\mathrm{f}} = \theta_{\mathrm{sl}} + \theta_{\mathrm{r}} \tag{26}$$

The reference torque and the flux-producing components of the current along with the field angle are converted into three-phase stationary reference frame using the inverse transformation to obtain three-phase reference currents given by the following equations.

$$i_{\mathrm{as}}^{*} = i_{\mathrm{ds}}\sin\theta + i_{\mathrm{qs}}\cos\theta \tag{27}$$

$$i_{\mathrm{bs}}^{*} = \left(\frac{1}{2}\right)\left\{-i_{\mathrm{ds}}\cos\theta + \sqrt{3}i_{\mathrm{ds}}\sin\theta\right\} + \left(\frac{1}{2}\right)\left\{i_{\mathrm{qs}}\sin\theta + \sqrt{3}i_{\mathrm{qs}}\cos\theta\right\} \tag{28}$$

$$i_{\mathrm{cs}}^{*} = -\left(i_{\mathrm{as}}^{*} + i_{\mathrm{bs}}^{*}\right) \tag{29}$$

The reference currents are compared with the main currents and processed by means of tolerance band current regulation to generate the switching pulses for the three legs of the voltage source inverter. The schematic of the sensorless drive system along with the modified observer is shown in Fig. 6.

4 Simulation Results

The sensorless drive system comprises of the induction motor, state observer, vector controller and the voltage source inverter. The ratings and the parameters of the motor used in the simulation study is given in the "Appendix." The motor along with the observer and controller is built using Simulink blocksets and run for the following test cases.

(i) Input DC-link voltage disturbance at constant speed of 120 radians per second (rps) and constant load of 100 Nm.
(ii) Step load variation (initially at no load, and after a fixed time interval of 5 s, 150 Nm) at a constant speed of 120 rps.
(iii) Step speed variation (initially at a speed of 50 rps, and after a fixed time interval of 5 s, 150 rps) at a constant load of 100 Nm.
(iv) At flux-weakening region (180 rps) at a constant load of 100 Nm.
(v) Low-speed operation (25 rps and 40 rps) at a constant load of 100 Nm.

4.1 Input DC-Link Voltage Disturbance

See Figs. 7, 8, 9 and 10.

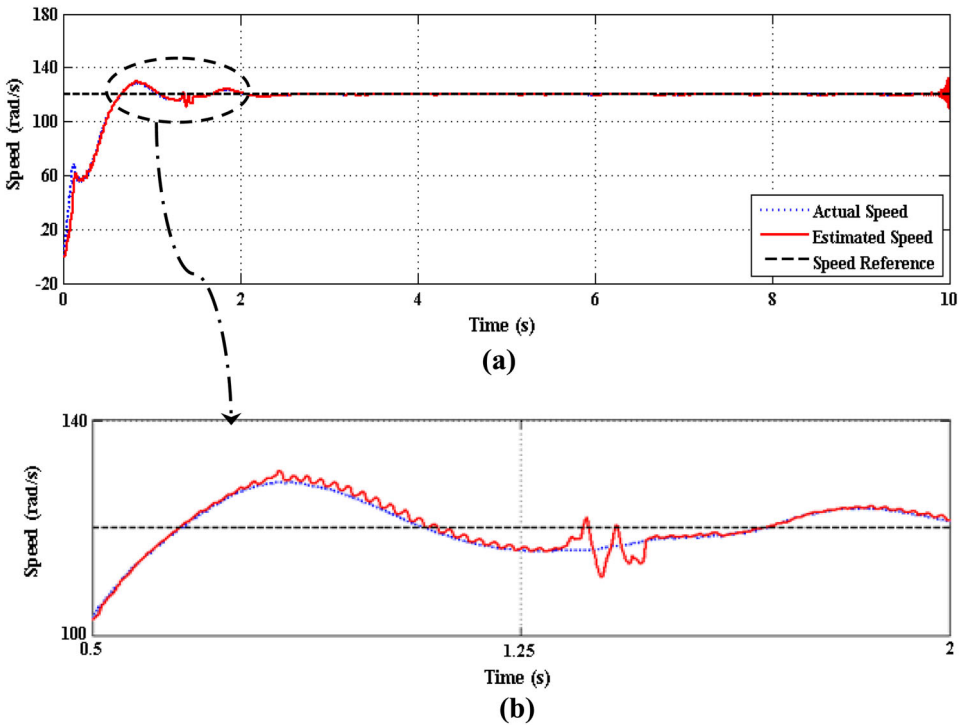

Fig. 7 **a** Estimated speed and **b** zoomed speed tracking of APRO 1

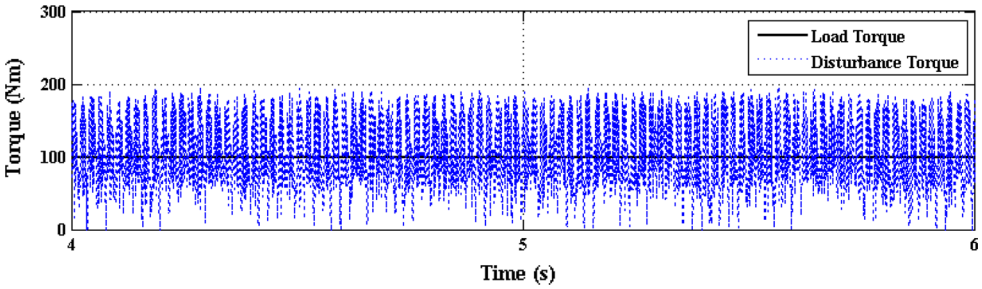

Fig. 8 Disturbance torque estimation of APRO 1

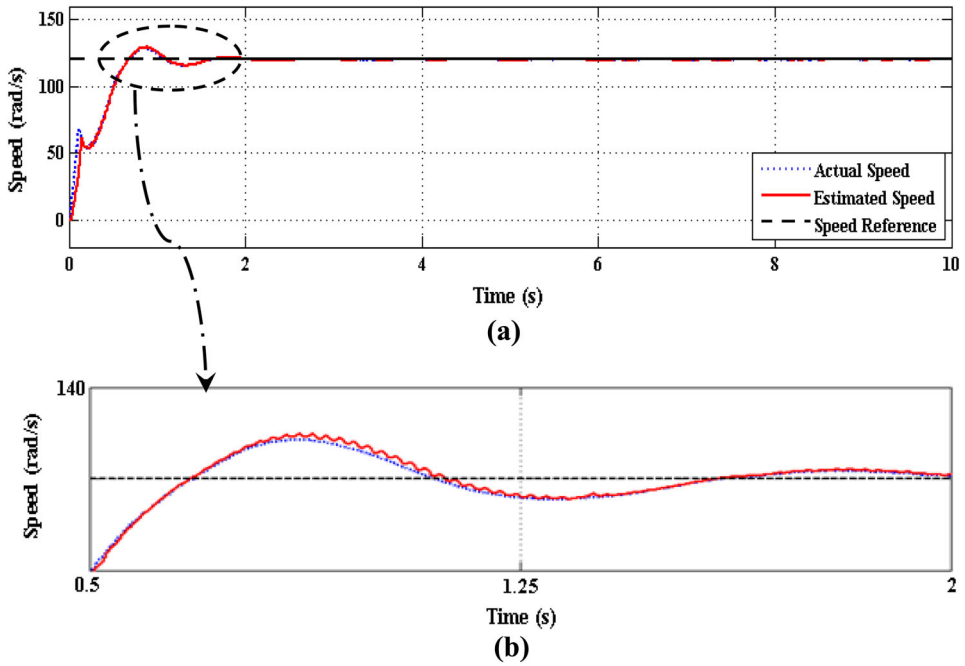

Fig. 9 **a** Estimated speed and **b** zoomed speed tracking of APRO 2

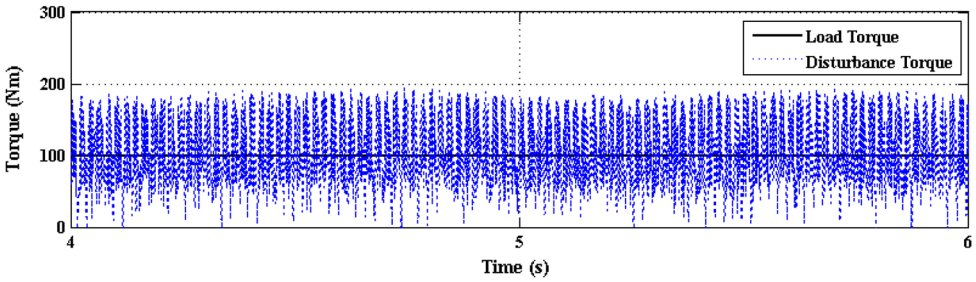

Fig. 10 Disturbance torque estimation of APRO 2

4.2 Step Load Variation

See Figs. 11, 12, 13 and 14.

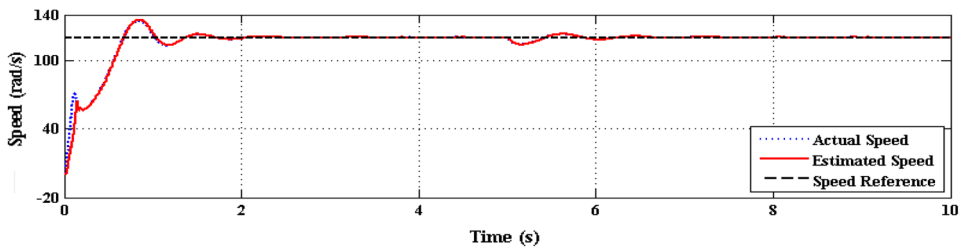

Fig. 11 Speed tracking of APRO 1

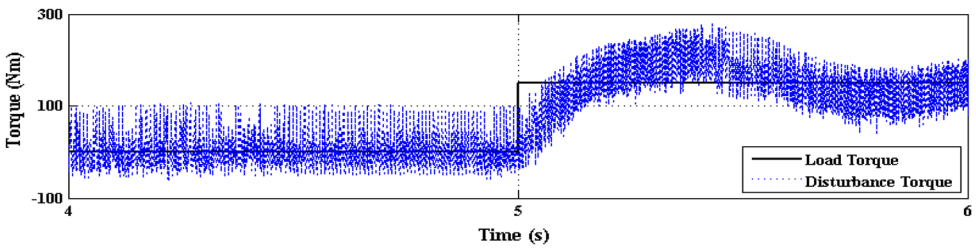

Fig. 12 Disturbance torque estimation of APRO 1

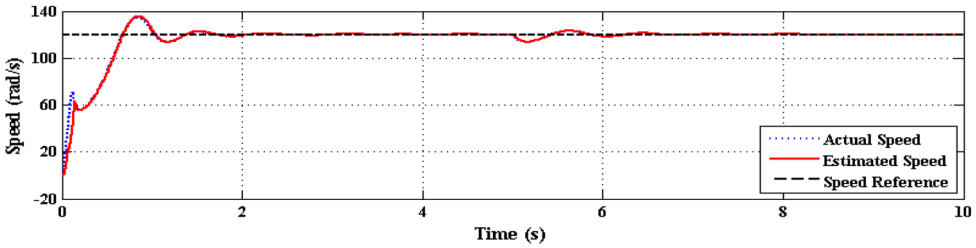

Fig. 13 Speed tracking of APRO 2

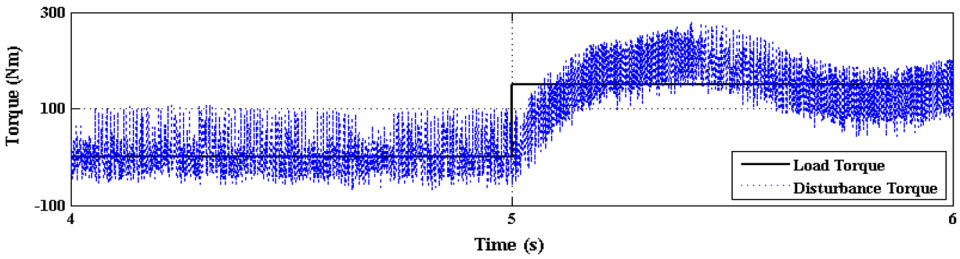

Fig. 14 Disturbance torque estimation of APRO 2

4.3 Step Speed Variation

See Figs. 15, 16, 17 and 18.

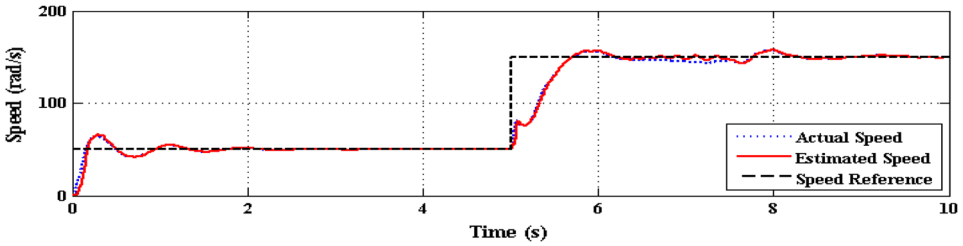

Fig. 15 Step speed command tracking of APRO 1

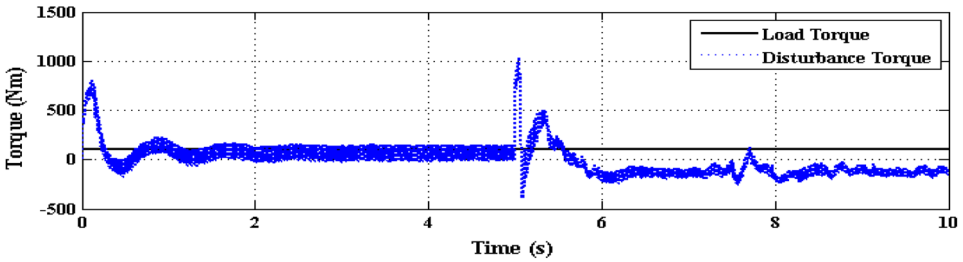

Fig. 16 Disturbance torque estimation of APRO 1

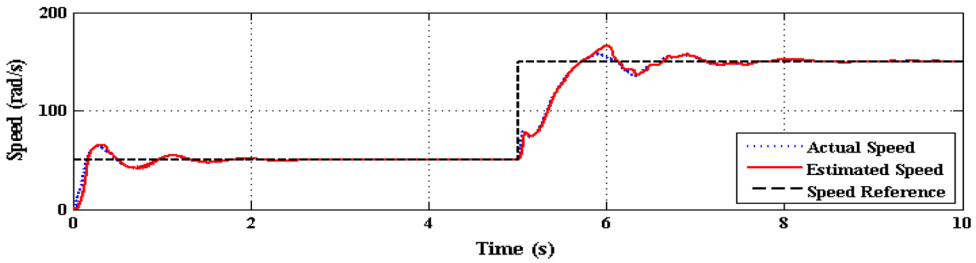

Fig. 17 Step speed command tracking of APRO 2

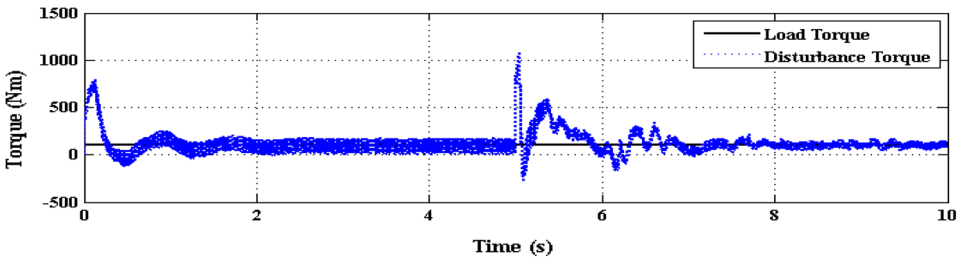

Fig. 18 Disturbance torque estimation of APRO 2

4.4 Flux-Weakening Mode

See Figs. 19, 20, 21 and 22.

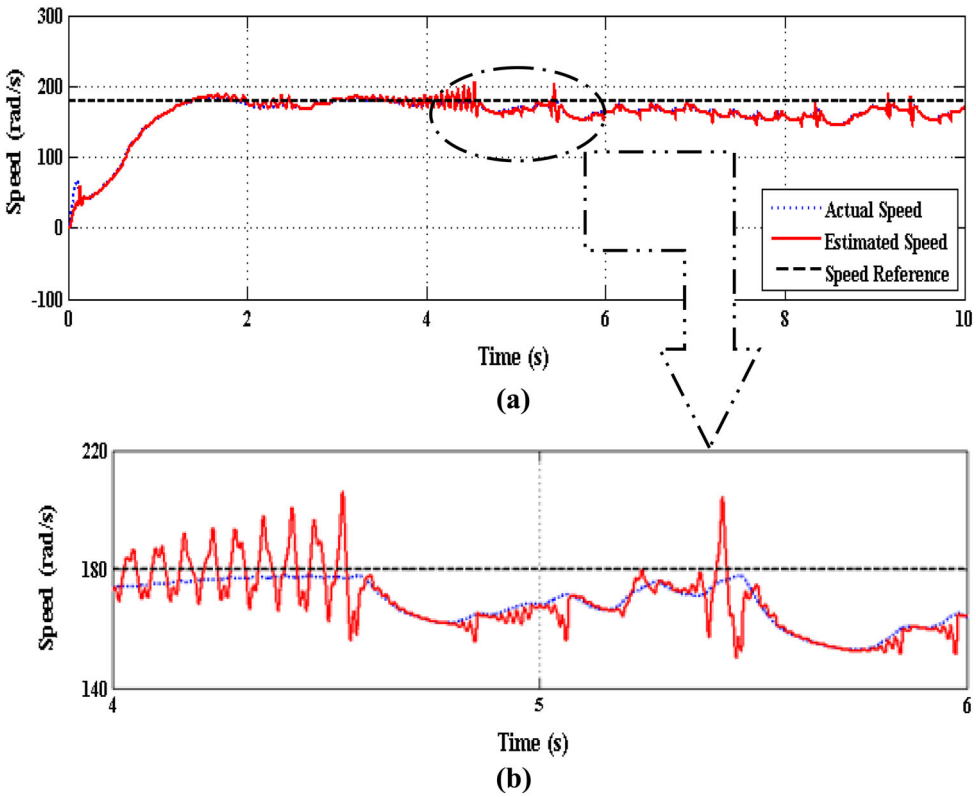

Fig. 19 **a** Estimated speed and **b** zoomed speed tracking of APRO 1

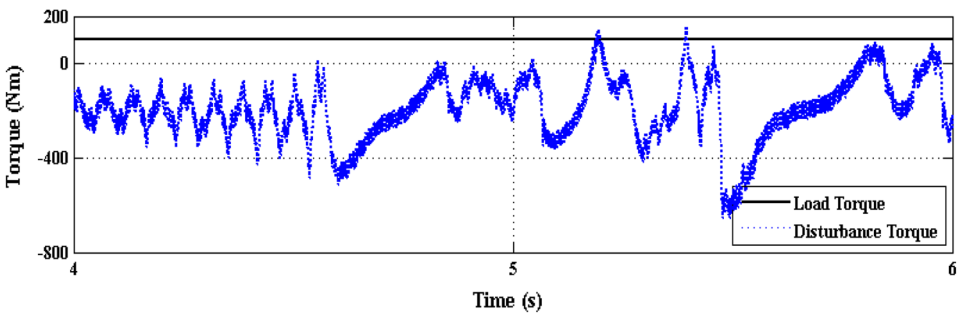

Fig. 20 Disturbance torque estimate of APRO 1

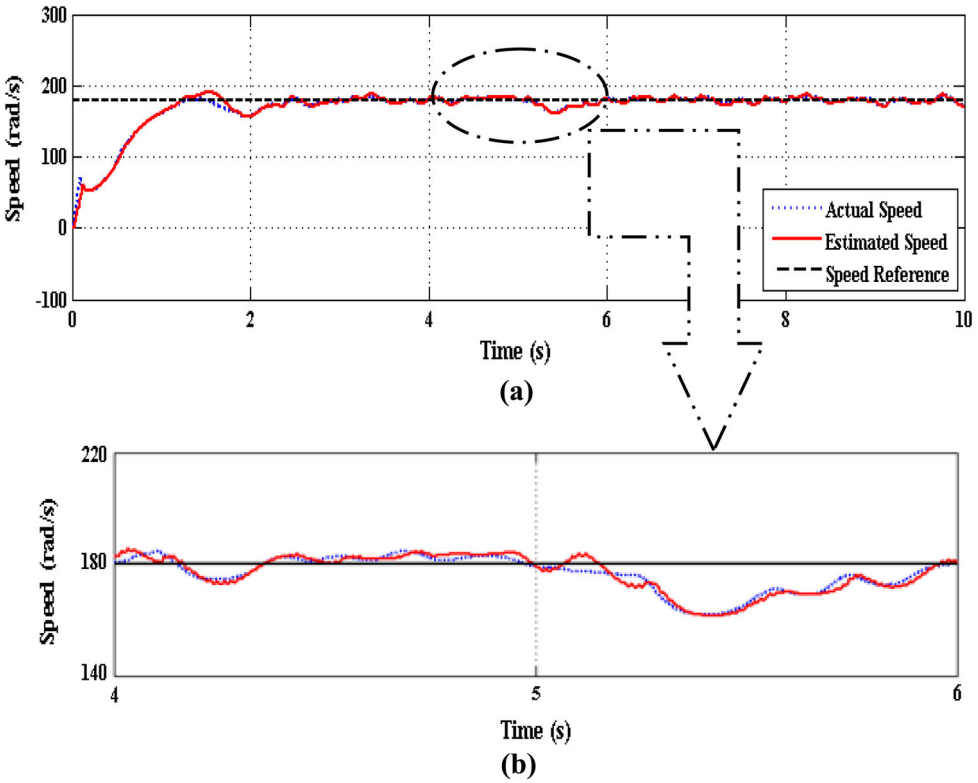

Fig. 21 **a** Estimated speed and **b** zoomed speed tracking of APRO 2

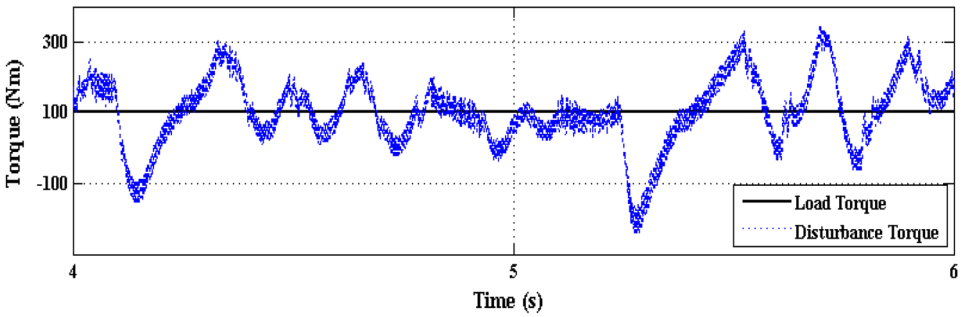

Fig. 22 Disturbance torque estimate of APRO 2

4.5 Low-Speed Operation

See Figs. 23, 24 and 25.

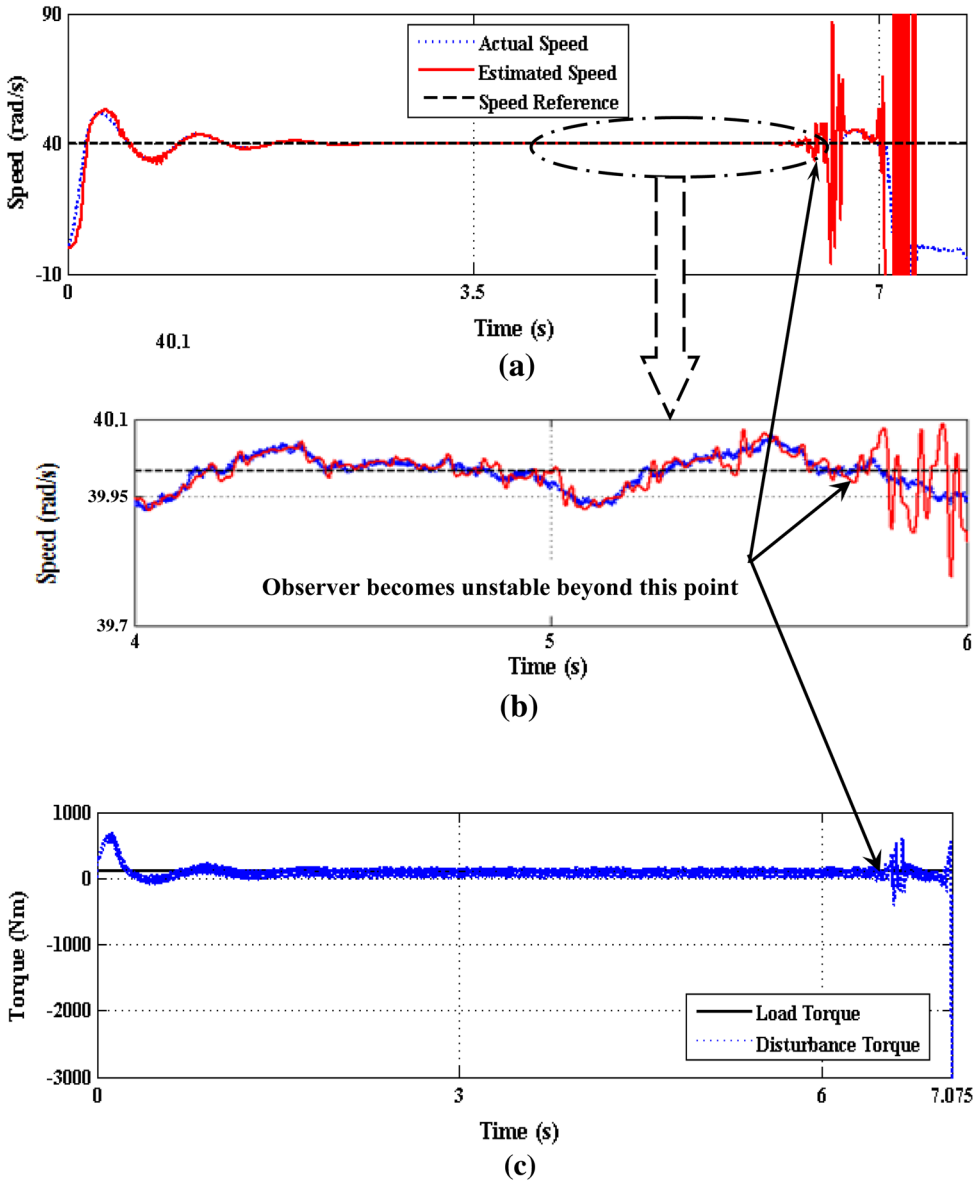

Fig. 23 **a** Estimated speed and **b** zoomed speed tracking of APRO 1. **c** Disturbance torque estimate of APRO 1

5 Discussion

The results of the simulation study are analyzed for each of the test cases. For the purpose of simplicity in analysis, APRO 1 is named as conventional observer and APRO 2 is named as modified observer. By superimposing an AC sine wave of 100 V amplitude on the DC-link voltage of magnitude 500 V, the input DC-link voltage disturbance is created. At constant speed and constant load, it is observed that the modified observer in Fig. 9a, b tracks the actual speed more smoothly compared to the conventional observer shown in Fig. 7a, b. This can be attributed to a superior disturbance rejection performance of the modified observer. The disturbance torque estimate is more or less the same for both the observers as shown in Figs. 8 and 10. For a step load perturbation at constant speed of 120 rps, both the observers exhibit similar performance in terms of disturbance estimation, as shown in Figs. 12 and 14. However, in terms of speed tracking, it can be seen that after 5 s, at rated load, the modified observer's settling time is faster in Fig. 13 as compared to the conventional observer shown in Fig. 11. For step variation in the speed command at constant load, the speed tracking of the conventional observer, although follows the profile of the actual speed, it takes more time to settle down (around 9.5 s) as shown in Fig. 15 as compared to the modified observer which settles down around 8.5 s but with a slightly higher peak overshoot, as shown in Fig. 17. Once again, the modified observer's ability to estimate and reject the disturbance shown in Fig. 18 is better compared to

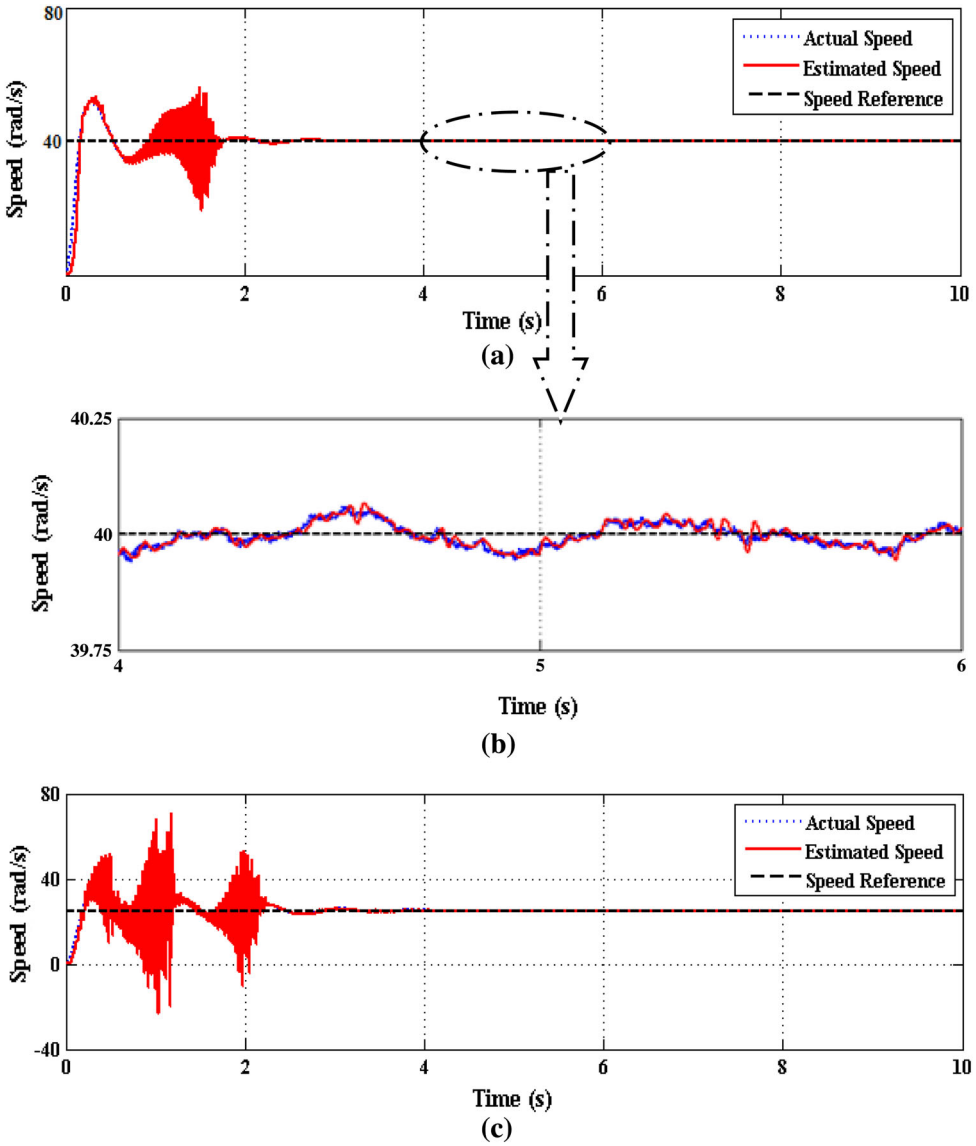

Fig. 24 **a** Speed tracking for 40 rps, **b** zoomed speed tracking for 40 rps, **c** speed tracking for 25 rps for APRO 2

the conventional observer which becomes unstable after 5 s as shown in Fig. 16.

During flux weakening, for the conventional observer, the speed tracking and disturbance estimation performance deteriorates heavily with high ripple content as shown in Figs. 19a, b and 20. However, in case of the modified observer, even though there are oscillations in estimated speed, the percentage of oscillations is comparatively less and a superior performance is observed as shown in Fig. 21a, b. The disturbance torque estimate also has lesser oscillations and averages the reference value as shown in Fig. 22. Finally, during low-speed operation at 40 rps, it can be distinctly seen that the speed and the disturbance torque estimation performance of the conventional observer become unstable and go out of bounds after 6.5 s as shown in Fig. 23a–c. But it is seen that the modified observer, for a full simulation time interval of 10 s, is stable and smooth although with an initial higher overshoot as shown in Figs. 24a, b and 25a. The conventional observer does not work for a speed command of 25 rps, whereas the modified observer works well even at this speed, once again, with an initial high peak overshoot as shown in Fig. 24c and a smoother disturbance torque estimate shown in Fig. 25b. The superiority of the modified observer with respect to different performance parameters for a particular test case of flux-weakening region (180 rps) is shown in Table 1.

6 Conclusions

The dynamic performances of two different disturbance rejection mechanisms in sliding mode state observer for sensorless vector-controlled induction motor drive are compared. It is inferred that the modified observer has more speed

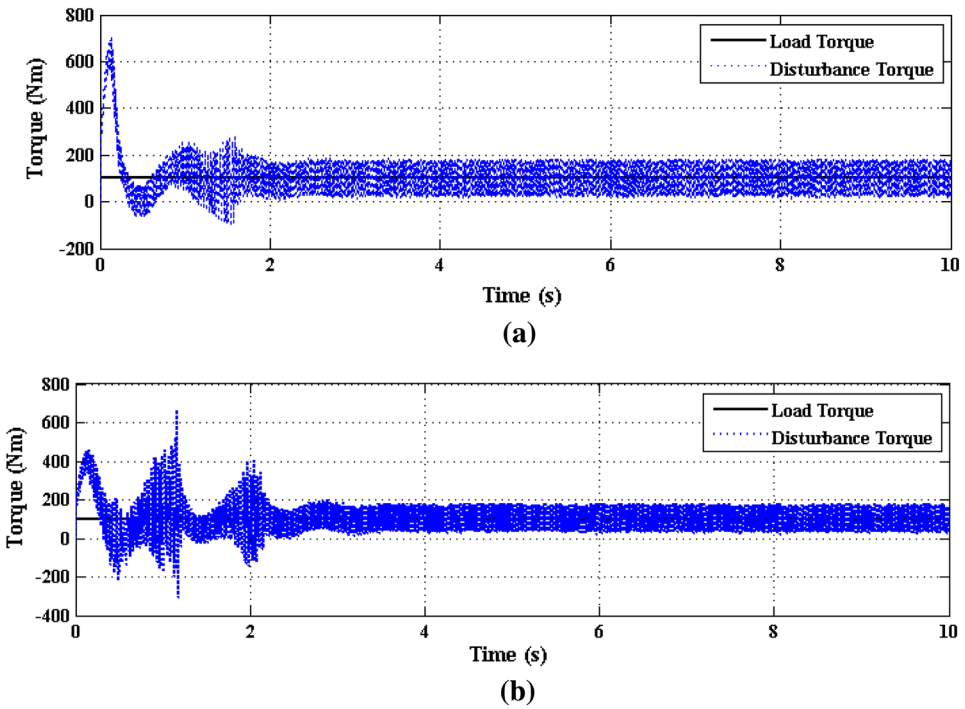

Fig. 25 **a** Disturbance torque estimate for 40 rps and **b** disturbance torque estimate for 25 rps for APRO 2

Table 1 Comparison of performance parameters

Performance parameters	APRO 1	APRO 2
Speed bandwidth	Works well in the 60–140 rps range	Works well in the 25–180 rps range
Settling time (for 120 rps speed command)	~ 2.5 s	~2 s
Steady state value (for flux weakening)	~ 165 rps	~ 183 rps
Maximum peak overshoot (for flux weakening)	~ 206 rps	~190.5 rps

bandwidth and comparatively better disturbance rejection. It also works well in the low speed range, which makes it suitable for sensorless motion control applications in the low speed range. In addition to it, the modified observer also performs well under the faulty operation mode, subjected to an electrical fault in the inverter, in the form of input DC-link voltage disturbance. This makes it also suitable for certain fault-tolerant control applications for induction motor.

Appendix

The motor ratings and the parameters considered for simulation are given as follows: a 50 HP, three-phase, 415 V, 50 Hz, star-connected, four-pole induction motor with equivalent parameters: $R_s = 0.087\,\Omega$, $R_r = 0.228\,\Omega$, $L_{ls} = L_{lr} = 0.8$ mH, $L_m = 34.7$ mH, inertia, $J = 1.662\,\text{kg m}^2$, friction factor = 0.1, viscous friction coefficient, $B_V = 0.1$.

References

1. Bose, B.K.: Modern Power Electronics and AC Drives. Prentice-Hall, New Delhi (1979)
2. Anitha, P.; Badrul, H.C.: Sensorless control of inverter-fed induction motor drives. Electr. Power Syst. Res. **77**(5–6), 619–629 (2007)
3. Ibrahim, A.; Idris, N.R.N.: A review on sensorless techniques for sustainable reliability and efficient variable frequency drives of induction motors. Renew. Sustain. Energy Rev. **24**, 11–21 (2013)
4. Zorgani, Y.A.; Koubaa, Y.; Boussak, M.: Simultaneous estimation of speed and rotor resistance in sensorless ISFOC induction motor drive based on MRAS scheme. XIX International Conference on Electrical Machines—ICEM 2010. Rome (2010)
5. Alexandru, T.; Gildas, B.: Observer scheme for state and parameter estimation in asynchronous motors with application to speed control. Eur. J. Control. **12**, 400–412 (2006)
6. Kojabadi, H.M.; Farouji, S.A.; Zarei, M.: A comparative study of various MRAS-based IM's rotor resistance adaptation methods. Iran J. Electr. Comp. Eng. **11**, 27–34 (2012)
7. Maiti, S.; Chakraborty, C.; Sengupta, S.: Simulation studies on model reference adaptive controller based speed estimation technique for the vector controlled permanent magnet synchronous motor drive. Simul. Model. Pract. Theory **17**, 585–596 (2009)
8. Lascu, C.; Boldea, I.; Blaabjerg, F.: A class of speed-sensorless sliding-mode observers for high-performance induction motor drives. IEEE Trans. Ind. Electron. **56**, 3394–3403 (2009)
9. Soto, G.G.; Mendes, E.; Razek, A.: Adaptive variable structure rotor flux observer for an induction motor. In: Power Electronics and Variable Speed Drives, pp. 318–323 (1998)
10. Comanescu, M.: An MRAS type estimator for the speed, flux magnitude and rotor flux angle of the induction motor using sliding

mode. In: International Symposium on Power Electronics, Electrical Drives, Automation and Motion (SPEEDAM 2014), pp. 719–724 (2014)
11. Vieira, R.P.; Gastaldini, C.C.; Azzolin, R.Z.; Grundling, H.A.: Discrete-time sliding mode speed observer for sensorless control of induction motor drives. IET Electr. Power App. **6**, 681–688 (2012)
12. Yongchang, Z.; Zhengming, Z.: Speed sensorless control for three-level inverter-fed induction motors using an extended luenberger observer. In: IEEE Vehicle Power and Propulsion Conference (VPPC), Harbin, China (2008)
13. Zhao, L.; Huang, J.; Liu, H.; Li, B.; Kong, W.: Second-order sliding-mode observer with online parameter identification for sensorless induction motor drives. IEEE Trans. Ind. Electron. **61**, 5280–5289 (2014)
14. Comanescu, M.; Xu, L.: Sliding-mode MRAS speed estimators for sensorless vector control of induction machine. IEEE Trans. Ind. Electron. **53**, 146–153 (2006)
15. Krzeminski, Z.: A new speed observer for control system of induction motor. In: IEEE International Conference on Power Electronics and Drive Systems, pp. 555–560 (1999)
16. Krzeminski, Z.: Observer of induction motor speed based on exact disturbance model. In: IEEE 13th International Power Electronics and Motion Control Conference, pp. 2294–2299 (2008)
17. Kubota, H.; Matsuse, K.: Robust field oriented induction motor drives based on disturbance torque estimation without rotational transducers. In: IEEE Industry Applications Society Annual Meeting, pp. 558–562 (1992)
18. Albu, M.; Horga, V.; Ratoi, M.: Disturbance torque observers for the induction motor drives. J. Electr. Eng. **6**, 1–6 (2006)
19. Zhiwu, H.; Yongteng, S.; Weihua, G.; Xiaohong, N.: Stability analysis and design of adaptive observer based on speed sensorless induction motor. In: IEEE Proceedings of the 26th Chinese Control Conference, pp. 28–32 (2007)
20. Mohan Krishna, S.; Febin Daya, J.L.: Effect of parametric variations and voltage unbalance on adaptive speed estimation schemes for speed sensorless induction motor drives. Int. J. Power Electron. Drive Syst. **6**, 77–85 (2015)
21. Slotine, J.J.E.; Li, W.: Applied Non-linear Control. Prentice-Hall, New Jersey (1998)
22. Comanescu, M.: Design and analysis of a sensorless sliding mode flux observer for induction motor drives. In: IEEE International Electric Machines and Drives Conference (IEMDC), pp. 569–574 (2011)